Effects of boson dispersion in fermion-boson coupled systems

Yukitoshi Motome
Institute of Materials Science, University of Tsukuba, Tsukuba, Ibaraki 305-0006, Japan

Gabriel Kotliar
Department of Physics, Rutgers University, Piscataway, New Jersey 08854-8019

(Received 23 May 2000)

We study the nonlinear feedback in a fermion-boson system using an extension of dynamical mean-field theory and the quantum Monte Carlo method. In the perturbative regimes (weak-coupling and atomic limits) the effective interaction among fermions increases as the width of the boson dispersion increases. In the strong-coupling regime away from the antiadiabatic limit, the effective interaction decreases as we increase the width of the boson dispersion. This behavior is closely related to complete softening of the boson field. We elucidate the parameters that control this nonperturbative region where fluctuations of the dispersive bosons enhance the delocalization of fermions.

I. INTRODUCTION

Interacting fermion-boson systems are very important in condensed matter physics and have been studied intensively.[1] They are directly relevant to the description of electron-lattice interaction. Other problems can be mapped onto interacting fermions and bosons by means of the Hubbard-Stratonovich transformation.[2,3] While the problem of a single fermion interacting with a boson field, i.e., the polaron problem, is well understood,[1] a lot less is known about the many-fermion problem in interaction with a boson field; it is a full interacting many-body problem that is tractable analytically only in the adiabatic[4] and the atomic limits.[5,6,1]

In this paper we revisit the interacting and dispersive fermion-boson problem using dynamical mean-field (DMF) theory.[7] This method reduces the quantum many-body problem to a quantum impurity model obeying a self-consistency condition. This method has been useful in describing strong-coupling problems such as the Mott transition. There are several motivations for our work.

First, a DMF treatment of the bosonic and fermionic degrees of freedom taking into account the boson dispersion requires an extension of the DMF equations where the bosonic propagator degrees of freedom are determined self-consistently. This represents a type of self-consistent DMF equation, that so far has not been investigated to our knowledge. These equations are relevant to many problems, electron-phonon interactions, fermions interacting with spin fluctuations[8] or among themselves via the long-ranged Coulomb interactions,[9] and to the boson-fermion model.[10]

Second, while the Mott transition in the Hubbard model is well understood using DMF methods, it is interesting to understand how it is modified by the variation of the frequency of the mode that mediates the interaction, or how the results are changed by the electron-phonon interactions. Competition and cooperation in the coexistence of interactions with different frequencies are also interesting.[11,12] The approach discussed in this paper is a step in this direction.

Finally, phonon dispersion effects are relevant to many systems. The Jahn-Teller or breathing-type phonons, for instance, seen in manganese oxides should be dispersive due to intersite coupling. A distortion of a MnO_6 octahedron affects distortions of the neighbor octahedra, since the MnO_6 octahedra share their oxygen atoms, which leads to an intersite coupling. This may be relevant to fascinating orderings of lattice and charge in doped manganites.[13–16]

We study the mutual feedback of fermionic and bosonic degrees of freedom in a very simple system of fermions interacting with one branch of bosons at half filling. However, the methodology can be extended to other problems where similar DMF equations occur, such as electron problems with long-ranged Coulomb interactions and the competition of magnetic order and the heavy fermion state, and to the boson-fermion mixture of high temperature superconductivity.

This paper is organized as follows. In the next section we discuss how DMF theory needs to be extended to fully include the feedback effects through fermion-boson interaction. The quantum Monte Carlo (QMC) method is introduced to solve the DMF equations in a wide region of parameters. We also discuss some technical points of the QMC method relevant to this problem. The formalism is applied to demonstrate effects of boson dispersion in a wide region of parameters and the results are summarized in Sec. III. In Sec. IV, we discuss our main result: the existence of two distinct regimes of the DMF solutions. In the first regime, the feedback effects increase the fermion-boson coupling. In the second regime, which is strongly fluctuating, the boson dispersion accelerates the delocalization of fermions. Complete softening of the boson fields characterizes the crossover between these regimes. Section V is devoted to a summary.

II. DYNAMICAL MEAN-FIELD FORMALISM AND HAMILTONIAN

In this work, we discuss feedback effects caused by the fermion-boson interaction using DMF theory. DMF theory provides a local view of a many-body problem in terms of an impurity model that satisfies a self-consistency condition.[7]

For general fermion-boson problems with a local interaction, the local action has the form

$$S_{\rm eff}=\int d\tau d\tau' \sum_{\alpha} c^{\dagger}_{\alpha}(\tau)\mathcal{G}^{-1}_{0\alpha}(\tau-\tau')c_{\alpha}(\tau') + \int d\tau d\tau' \sum_{\nu} x_{\nu}(\tau)\mathcal{D}^{-1}_{0\nu}(\tau-\tau')x_{\nu}(\tau') + \int d\tau \sum_{\alpha_1\alpha_2\nu} \lambda_{\alpha_1\alpha_2\nu}c^{\dagger}_{\alpha_1}(\tau)c_{\alpha_2}(\tau)x_{\nu}(\tau), \quad (1)$$

where $\mathcal{G}_0$ and $\mathcal{D}_0$ are the bare impurity Green's functions for fermion and boson, respectively, which contain the integrated dynamical information of the other sites. Here c_α is the fermion annihilation operator and x_ν is the boson field. $\lambda_{\alpha_1\alpha_2\nu}$ denotes the coupling between fermions and bosons. The index α (ν) denotes internal degrees of freedom of fermions (bosons) such as spins or orbitals of electrons (normal modes of phonons). We do not explicitly write the contribution from fermion interactions such as the Coulomb interaction since we focus on the effects of boson dispersions in this paper. However, the action (1) is quite general and contains such fermion interactions through the Hubbard-Stratonovich transformation[2,3] with continuous fields. Of course, alternatively, one can include additionally the fermion interactions according to the DMF theory for Hubbard-type models.[7]

The full Green's functions are related to the bare ones by

$$\mathcal{G}^{-1}_{\alpha}(i\omega_n)=\mathcal{G}^{-1}_{0\alpha}(i\omega_n)-\Sigma_{\alpha}(i\omega_n), \quad (2)$$

$$\mathcal{D}^{-1}_{\nu}(i\omega_n)=\mathcal{D}^{-1}_{0\nu}(i\omega_n)-\Pi_{\nu}(i\omega_n), \quad (3)$$

at each Matsubara frequency $\omega_n=(2n+1)\pi/\beta$ for fermions and $\omega_n=2n\pi/\beta$ for bosons, respectively (n is an integer). β is the inverse temperature. Σ and Π are the self-energy for fermions and bosons, respectively. The Green's functions for both fermions and bosons are determined in a self-consistent way. This is achieved by the following set of self-consistency conditions:

$$\mathcal{G}_{\alpha}=\sum_{\mathbf{q}} [i\omega_n+\mu-\epsilon_{\mathbf{q}\alpha}-\Sigma_{\alpha}(i\omega_n)]^{-1}, \quad (4)$$

$$\mathcal{D}_{\nu}=\sum_{\mathbf{q}} [(i\omega_n)^2-\omega^2_{\mathbf{q}\nu}-\Pi_{\nu}(i\omega_n)]^{-1}, \quad (5)$$

where $\epsilon_{\mathbf{q}\alpha}$ and $\omega_{\mathbf{q}\nu}$ give the dispersion relations for fermions and bosons, respectively, as a function of the wave number $\mathbf{q}$. μ is the chemical potential to control the density of fermions. Here the bosons are described as harmonic oscillators. The condition (5) is modified according to the boson degrees of freedom.

Previous studies of other models have indicated that the results of the DMF theory can give useful insights into three-dimensional systems.[7] We therefore take the dispersions $\epsilon_{\mathbf{q}}$ and $\omega_{\mathbf{q}}$ that correspond to a semicircular density of states (see the details in Sec. III A). These DMF equations are exact for a model where the fermions and bosons have random hopping on lattice sites.

The self-consistency loop is closed as follows: The effective action (1) is solved for given bare impurity Green's functions $\mathcal{G}_0$ and $\mathcal{D}_0$ to obtain the full Green's functions $\mathcal{G}$ and $\mathcal{D}$. The self-energy Σ and Π are calculated by the relations (2) and (3), and used to obtain the Green's functions through the self-consistency conditions (4) and (5). New bare impurity Green's functions are calculated by the relations (2) and (3) again. This loop is iterated until all the quantities are converged. In this way, both fermionic and bosonic dispersions are renormalized through the fermion-boson interaction, and the mutual feedback effects are fully included.

The above DMF equations assume that no symmetry breaking is present in the system although the extension to phases with broken symmetry is straightforward. The equations can be derived from a fermion-boson coupled model:

$$\mathcal{H}=\mathcal{H}_{\rm F}+\mathcal{H}_{\rm B}+\mathcal{H}_{\rm I}, \quad (6)$$

where

$$\mathcal{H}_{\rm F}=\sum_{\alpha}\sum_{ij} t^{\alpha}_{ij}c^{\dagger}_{i\alpha}c_{j\alpha}-\mu\sum_{\alpha i} c^{\dagger}_{i\alpha}c_{i\alpha}, \quad (7)$$

$$\mathcal{H}_{\rm B}=\frac{1}{2}\sum_{\nu}\left(\sum_{i}\frac{p^2_{i\nu}}{M_{\nu}}+\sum_{ij} M_{\nu}\omega^2_{ij\nu}x_{i\nu}x_{j\nu}\right), \quad (8)$$

$$\mathcal{H}_{\rm I}=\sum_{\alpha_1\alpha_2\nu}\sum_{i}\lambda_{\alpha_1\alpha_2\nu}c^{\dagger}_{i\alpha_1}c_{i\alpha_2}x_{i\nu}. \quad (9)$$

Here $p_{i\nu}$ is the conjugate momentum of the boson coordinate $x_{i\nu}$, and M_ν is the boson mass of the mode ν.

The model (6) has been intensively studied using DMF methods in the limit of zero boson dispersion, i.e., in the Holstein model.[5,6] Bosons with the same index ν have the same frequency (Einstein phonons) as

$$\mathcal{H}_{\rm B}=\frac{1}{2}\sum_{\nu i}\left(\frac{p^2_{i\nu}}{M_{\nu}}+M_{\nu}\omega^2_{0\nu}x^2_{i\nu}\right), \quad (10)$$

where the index i denotes a lattice site. In the ground state, the possibility of charge-ordered or superconducting states has been intensively discussed for this model.[17–21] Above the critical temperatures of these states, crossover behavior is observed from the Fermi liquid with a mass enhancement in the weak-coupling region to the so-called polaron, which is a combined object of fermions and bosons in the strong-coupling region.[1,5,6,22]

It is instructive to compare the present framework with the DMF theory for the problem without boson dispersion, such as the Holstein model. If bosons have no dispersion, that is, all $\omega_{\mathbf{q}}$ take the same value ω_0 independent of $\mathbf{q}$, Eq. (5) is rewritten as

$$\mathcal{D}=[(i\omega_n)^2-\omega^2_0-\Pi(i\omega_n)]^{-1}. \quad (11)$$

Although the full Green's function $\mathcal{D}$ contains a feedback effect in the self-energy Π, the bare impurity Green's function $\mathcal{D}_0$ is fixed at the noninteracting Green's function given by

$$\mathcal{D}^{\rm free}_0=[(i\omega_n)^2-\omega^2_0]^{-1} \quad (12)$$

throughout the self-consistency iterations when we start from $\mathcal{D}_0=\mathcal{D}^{\rm free}_0$. This is equivalent to the ordinary DMF theory for the Holstein model which does not need Eqs. (3) and

(5).[21,22] Compared to this, for the cases with finite bosonic dispersion, the bare impurity Green's function $\mathcal{D}_0$ is renormalized from $\mathcal{D}_0^{\rm free}$ in the iterations in our formalism.

The renormalization of $\mathcal{D}_0$ plays a crucial role because $\mathcal{D}_0$ is related to the effective interaction between fermions. If we integrate out the boson variables x, the effective interaction between fermions takes the form

$$\sum_{\alpha_1\alpha_2\alpha_3\alpha_4} \int d\tau\, d\tau'\, c^\dagger_{\alpha_1}(\tau) c_{\alpha_2}(\tau) U_{\rm eff}(\tau-\tau') c^\dagger_{\alpha_3}(\tau') c_{\alpha_4}(\tau'), \tag{13}$$

where

$$U_{\rm eff}(\tau) = \lambda^2 \mathcal{D}_0(\tau). \tag{14}$$

In the absence of boson dispersion, since $\mathcal{D}_0$ is unchanged through the self-consistency loop as mentioned above, the effective interaction (14) is also unrenormalized. On the other hand, $\mathcal{D}_0$ is renormalized in our formalism for finite dispersion, which means that the effective interaction between fermions is renormalized by the mutual feedback of the fermion-boson coupling.

There are several techniques for solving the effective impurity problem with the action (1). In this work, we employ the QMC method[7,23] because it is an unbiased calculation and suitable for investigating a wide region of parameters beyond the perturbative regimes.[24] In the QMC approach, the imaginary time is discretized into L slices with the width $\Delta\tau$ $(\Delta\tau=\beta/L)$. Continuous variables $x_{\nu l}=x_\nu(\tau_l)$ $(\tau_l=l\Delta\tau, l=1,2,\ldots,L)$ are randomly updated to $x'_{\nu l}$ with the probability

$$\prod_\alpha \frac{\det \mathcal{G}_\alpha}{\det \mathcal{G}'_\alpha} \frac{\exp[-\Delta\tau B(x'_{\nu l})]}{\exp[-\Delta\tau B(x_{\nu l})]}, \tag{15}$$

where $B(x_{\nu l})=\sum_{j=1}^L x_{\nu j} \mathcal{D}^{-1}_{0\nu jl} x_{\nu l}$ with $\mathcal{D}_{0\nu jl}=\mathcal{D}_{0\nu}(\tau_j-\tau_l)$. The fermion Green's functions $\mathcal{G}$ and $\mathcal{G}'$ are calculated by the standard algorithm[23] for the configurations with $x_{\nu l}$ and $x'_{\nu l}$, respectively.

In actual QMC samplings, we consider both local and global updates for the continuous fields $x_{\nu l}$. The local update consists of sequential updates of the fields on each discretized point; a change from $x_{\nu l}$ to $x'_{\nu l}=x_{\nu l}+r\delta$ is attempted, where r is a random number between -1 and 1 and δ is a given amplitude. The global update is a simultaneous movement of all the fields by the same amount $r\delta$. The latter becomes important especially in the strong-coupling region and/or at low temperatures where the fields x show some ordering or are nearly ordered. The update amplitude δ is chosen to give an appropriate value of the acceptance ratio, which is defined as the ratio of the number of accepted samples to the total number of trials.

QMC calculations generally have a negative sign problem; the MC weight (15) can be negative for the general action (1), which leads to numerical instability in the QMC measurements. However, if fermions couple to bosons only in the diagonal form, that is, the coupling parameter $\lambda_{\alpha_1\alpha_2\nu}$ is nonzero only for the case of $\alpha_1=\alpha_2$, the MC weight (15) becomes positive definite.[25] In this case, there is no negative sign problem.

There are two sources of error in the QMC calculations. One is a systematic error due to the discretization of the imaginary time, and the other is a statistical error from the random sampling. The former error is known to be proportional to $(\Delta\tau^2)$. Measurement is divided into several bins to estimate the latter statistical error by variance among the bins. The magnitude of each error depends on the specific form of model and parameters.

III. RESULTS

A. Model and parameters

We apply the DMF framework proposed in the previous section to the case where the general Hamiltonian (6) contains two species of fermions and one branch of bosons. We set the mass $M=1$. The model is a straightforward extension of the Holstein model to include dispersive bosons, whose fermion-boson interaction is explicitly given by

$$\mathcal{H}_{\rm I} = -\lambda \sum_i \sum_{\alpha=1,2} \left(c^\dagger_{i\alpha} c_{i\alpha} - \frac{1}{2} \right) x_i, \tag{16}$$

where the index α takes two values, like the spin degrees of freedom of electrons. The interaction is diagonal in the fermion index α so that the QMC method does not suffer from the negative sign problem mentioned in Sec. II. The term (16) favors a doubly occupied or an empty state on each site. Note that the model has particle-hole symmetry at $\mu=0$.

The boson dispersion is taken into account through Eq. (5) in the present framework. We replace the summations over the wave number $\mathbf{q}$ in Eqs. (4) and (5) by energy integrations as

$$\mathcal{G}(i\omega_n) = \int \frac{D_{\rm F}(\varepsilon)d\varepsilon}{i\omega_n+\mu-\varepsilon-\Sigma(i\omega_n)}, \tag{17}$$

$$\mathcal{D}(i\omega_n) = \int \frac{D_{\rm B}(\varepsilon)d\varepsilon}{(i\omega_n)^2-\varepsilon^2-\Pi(i\omega_n)}, \tag{18}$$

where $D_{\rm F}$ and $D_{\rm B}$ are the the densities of states for fermions and bosons, respectively. In the following calculations, we assume a semicircular density of states as

$$D_{\rm F}(\varepsilon) = \frac{2}{\pi W^2}\sqrt{W^2-\varepsilon^2}, \tag{19}$$

$$D_{\rm B}(\varepsilon) = \frac{2}{\pi \omega_1^2}\sqrt{\omega_1^2-(\varepsilon-\omega_0)^2}, \tag{20}$$

where W is the half bandwidth of the fermion density, of states, which is taken as unity hereafter $(W=1)$; ω_0 and ω_1 are the center and the half bandwidth of the boson density of states, respectively $(\omega_0>0,\ \omega_0-\omega_1>0)$. For a semicircular density of states, the integrations (17) and (18) are performed analytically[7] and give

$$\mathcal{G} = \frac{\zeta-\sqrt{\zeta^2-4t^2}}{2t^2}, \tag{21}$$

$$\mathcal{D}=\frac{1}{\xi}\left[\frac{1}{\xi_-+\sqrt{\xi_-^2-\omega_1^2}}+\frac{1}{\xi_++\sqrt{\xi_+^2-\omega_1^2}}\right], \qquad (22)$$

where $\zeta=i\omega_n+\mu$ and $\xi_\pm=\xi\pm\omega_0$ with $\xi^2=(i\omega_n)^2-\Pi$.

The shape of the boson density of states near the bottom is important because bosons at the band edge can be easily excited and interact strongly with fermions. The semicircular density of states (20) has an $\varepsilon^{1/2}$ singularity, which is expected for bosons with ordinary cosine dispersions in three dimensions. Therefore we believe that the following results are qualitatively unchanged in realistic three-dimensional models. Results would be different for the two-dimensional density of states, which has a step discontinuity at the band edges and results in very different DMF solutions.

In the absence of the boson dispersion ($\omega_1=0$), the model with the interaction (16) (the ordinary Holstein model) shows a charge ordering around half filling ($\mu=0$) and superconductivity in doped regions at very low temperatures.[17–21] In the following, we examine the effects of boson dispersion in the low temperature region above and around these transition temperatures at half filling ($\mu=0$) assuming no symmetry breaking. The calculations are mainly performed at $\beta=8$. We take $\Delta\tau=1/4$, for which all the measured quantities are converged to the limit of $\Delta\tau\rightarrow 0$ within the statistical errors. We have typically run 1 000 000 MC steps for measurements; one MC sampling means a set of a sweep of local updates over all the discretized points and a global update. Convergence in the self-consistency loop is usually rapid; typically 10 iterations are required to converge within the statistical error bars when we start from the noninteracting Green's functions. However, in the strong-coupling case, the iteration often suffers from an oscillation between two solutions. To avoid the oscillation, we make the iteration proceed by mixing the previous solutions.

B. Dispersionless boson

First, we reconsider the limit without boson dispersion, that is, $\omega_1=0$. In this case, we use the two parameters ω_0 and $U=\lambda^2/M\omega_0^2$ to characterize the basic properties of the system. The first parameter ω_0 describes the adiabaticity. In the adiabatic limit of $\omega_0\rightarrow 0$, the boson fields do not change in imaginary time, that is, they behave as classical fields. In the opposite limit of $\omega_0\rightarrow\infty$, the bosons react instantaneously to fermion motion. Between these two limits, bosons with a finite ω_0 mediate a retarded effective interaction which is given by $U_{\rm eff}$ in Eq. (14). The second parameter U describes the magnitude of the effective interaction between fermions. Note that $U=|U_{\rm eff}(\omega_n=0)|$ in this dispersionless case, since the bare impurity Green's function is given by the noninteracting one (12).

For a fixed value of ω_0, the system behaves quite differently in the regions with $U\ll 1$ and $U\gg 1$. For small values of U, fermions are nearly free and each lattice site is in an empty, a singly occupied, or a doubly occupied state with almost equal probability at half filling ($\mu=0$). If we define the probability $P(x)$ that the boson field x lies in the interval between x and $x+\Delta x$, $P(x)$ shows a single broad peak centered at $x=0$. Compared to this, if U becomes large, fermions strongly interact with each other to form a combined state between fermion and boson, which is called a polaron. The polaron consists of double occupancy of fermions for the model with the interaction (16) (bipolaron). Thus, the probability $P(x)$ displays a double peak at $x=\pm\lambda/M\omega_0^2$, which corresponds to the doubly occupied and empty states. Figure 1 shows this behavior by changing the value of U for the case of $\omega_0=0.5$. The single peak of the probability $P(x)$ appears for small U, while the double peaks are developed for $U\gtrsim 1$ as shown in Fig. 1(a). At the same time, in Fig. 1(b), the probability of double occupancy $P_{\rm D}$ increases from 1/4 for the noninteracting case to 1/2 for the situation in which the system consists of only empty and doubly occupied sites. The self-energy for fermions Σ is also enhanced by the effective interaction between fermions U. Figure 1(c) shows that the absolute value of the imaginary part of the self-energy as a function of Matsubara frequency is strongly enhanced by U. Note that the data for $\omega_n>1/\Delta\tau$ contain no unbiased information. These clearly indicate the crossover from weakly correlated fermions in the small U region to polarons in the large U region.[22]

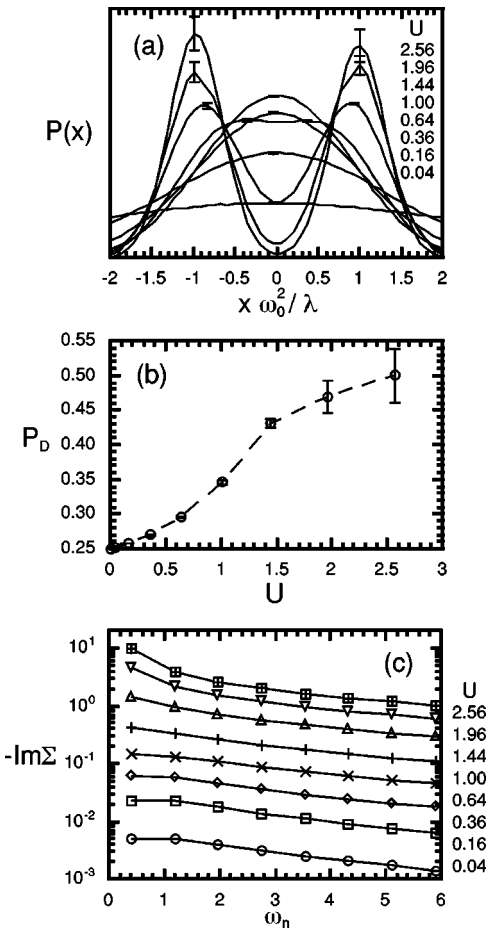

FIG. 1. Results for the dispersionless model with $\omega_0=0.5$ at $\beta=8$; (a) the probability function of the boson fields x, (b) the probability of double occupancy, and (c) the imaginary part of the self-energy for fermions as a function of Matsubara frequency. In (a), the typical error bars are shown at the peaks of the distributions. The lines in (b) and (c) are guides to the eye.

A similar crossover is found for other values of ω_0. Figures 2 and 3 show the results for $\omega_0=2$ and 8, respectively. The value of U for the crossover, which we call U^* hereaf-

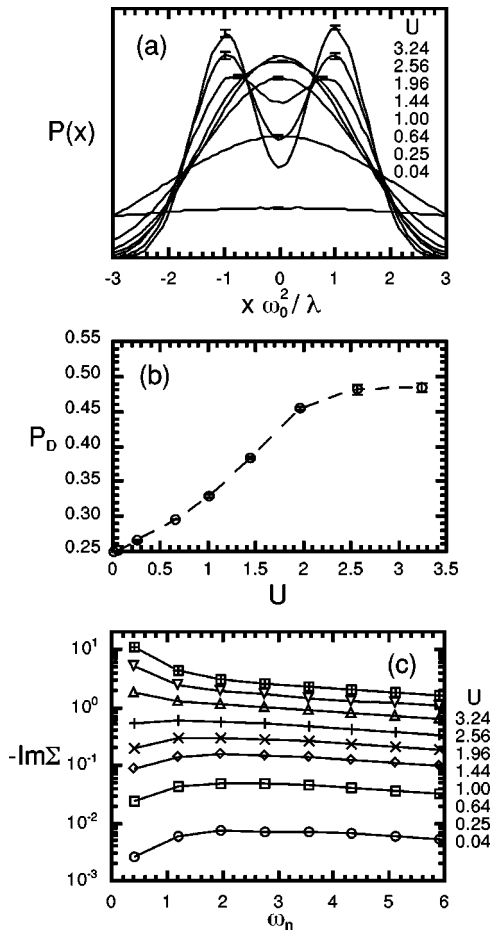

FIG. 2. Results for the dispersionless model with $\omega_0=2$.

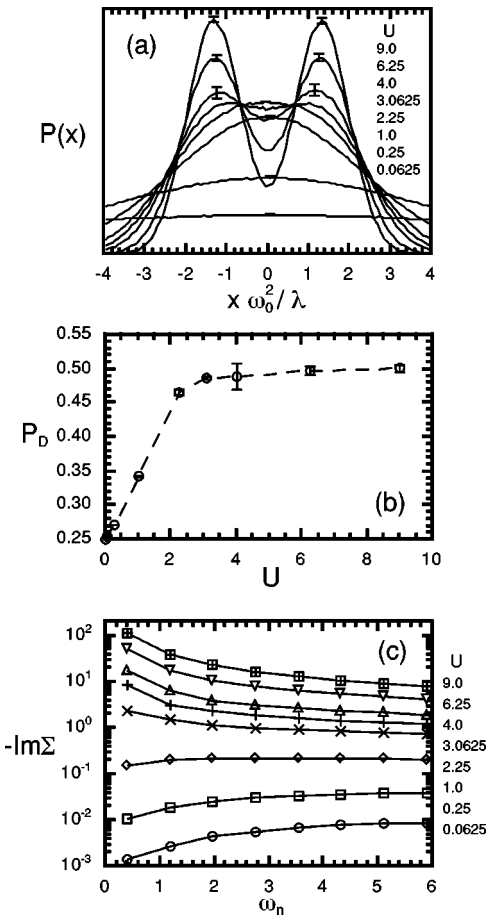

FIG. 3. Results for the dispersionless model with $\omega_0=8$.

ter, depends on the value of ω_0. For example, for the case of $\omega_0=0.5$ in Fig. 1, the double-peak structure of $P(x)$ appears at $U\sim 1$; on the other hand, it does not appear up to $U\sim 3$ for $\omega_0=8$. This can be understood as follows: In the limit of $\omega_0\to\infty$, since the effective interaction becomes spontaneous, $U_{\rm eff}(\tau)=-U\delta(\tau)$, the model maps onto an attractive Hubbard model[26] in which the boson field corresponds to the continuous Hubbard-Stratonovich field.[2,3] In the Hubbard model, it is known that the continuous field develops a double-peak distribution at $U\sim 3$, which corresponds to the opening of the Hubbard gap in the case of a repulsive interaction.[7] On the other hand, in the opposite limit of $\omega_0\to 0$, the effective interaction becomes constant in imaginary time, $U_{\rm eff}(\tau)=-U$. This case is identical to an attractive Falicov-Kimball model in the limit of a continuous number of configurations for the static fields.[21] In the adiabatic limit, the fermions are localized at a smaller value of U since fluctuation of the boson field is smaller in this case than in the antiadiabatic limit. Thus the splitting of the distribution of x should appear at a lower value of U. In the Falicov-Kimball model with a discrete static field, the critical value of U is estimated to be 1.[27,28] The finite value of ω_0 can interpolate between these two limits. Thus the value of U^* may change smoothly from $U^*\sim 3$ in the limit of $\omega_0\to\infty$ to $U^*\sim 1$ in the limit of $\omega_0\to 0$. This crossover will be discussed in the phase diagrams in Sec. IV.

C. Dispersive boson: weak-coupling limit

Now we discuss the cases with finite bosonic dispersion; $\omega_1\neq 0$. First, we study the weak-coupling limit of $W\gg\omega_0$ and U that has been studied by perturbation theory.[4]

In this region, the finite width of the boson dispersion ω_1 enhances the effective interaction between fermions. Figure 4(a) shows the bare impurity Green's function for bosons $\mathcal{D}_0$ as a function of Matsubara frequency for various values of ω_1 for the case of $\omega_0=0.5$ and $U=0.16$ ($\lambda=0.2$). $\mathcal{D}_0$ is enhanced by the width of the dispersion ω_1, which indicates that, through the relation (14), the effective interaction between fermions $U_{\rm eff}$ is enhanced by ω_1. This enhancement is also observed in the imaginary part of the fermion self-energy as shown in Fig. 4(b). At the same time, the probability of double occupancy becomes large as shown in Fig. 4(c). These features are similar to those in Figs. 1–3 when the parameter U increases in the small U region. These results can be understood using a perturbative argument (Sec. IV).

D. Dispersive boson: atomic limit

Next, we consider the limit of $W\ll\omega_0$ and U, which has been studied based on so-called small-polaron theory.[5,6,1] In this limit, the coherent band motion of fermions in Eq. (7) is a perturbation of other terms of Eqs. (8) and (9). The small polaron theory is a perturbative approach from the atomic limit. The strong interaction between fermions and bosons

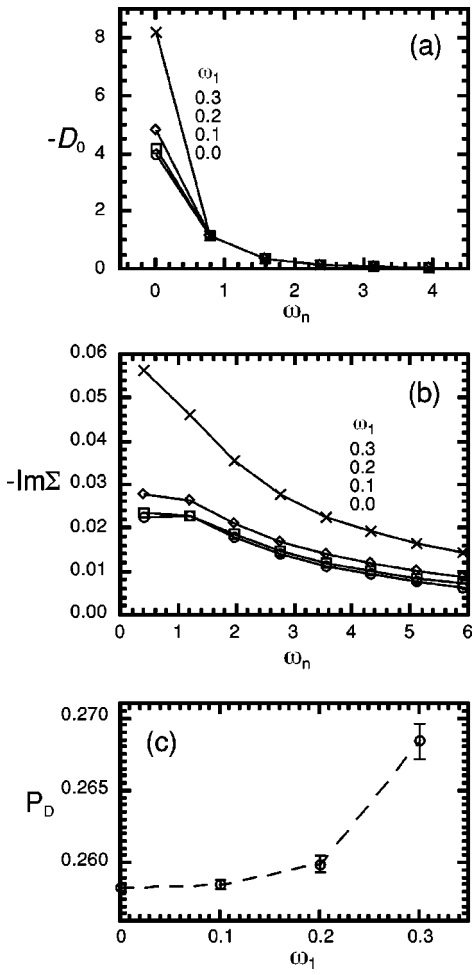

FIG. 4. Results for the dispersive boson model in the weak-coupling regime with $\omega_0=0.5$ and $U=0.16$ ($\lambda=0.2$) at $\beta=8$; (a) the bare impurity Green's function for bosons as a function of Matsubara frequency, (b) the imaginary part of the self-energy for fermions, and (c) the probability of double occupancy as a function of the width of the boson dispersion. The lines are guides to the eye.

leads to the formation of the small polaron state as mentioned in the dispersionless case in Sec. III B.

In this region, as in the weak-coupling case in Sec. III C, the effective interaction between fermions is enhanced by the finite width of the boson dispersion. Figure 5(a) plots the bare impurity Green's function for bosons at zero Matsubara frequency for $\omega_0=8$ and $U=9$ ($\lambda=24$). A finite width of the boson dispersion ω_1 enhances $\mathcal{D}_0(\omega_n=0)$. $\mathcal{D}_0$ shows the largest change at zero frequency, as in Fig. 4(a). At the same time, the absolute value of the imaginary part of the fermion self-energy increases as shown in Fig. 5(b). We plot here the data at the smallest Matsubara frequency to show the behavior clearly. The double-peak structure of the probability function $P(x)$ shown in Fig. 3(a) at $\omega_1=0$ does not change for ω_1 within statistical error bars. This suggests that the finite width of the boson dispersion enhances the effective interaction while the polaron state remains stable. These features will be discussed based on small polaron theory in Sec. IV.

E. Dispersive boson: strong-fluctuation regime

Here we go beyond the perturbative regimes studied in Secs. III C and III D. We consider the strong-coupling case

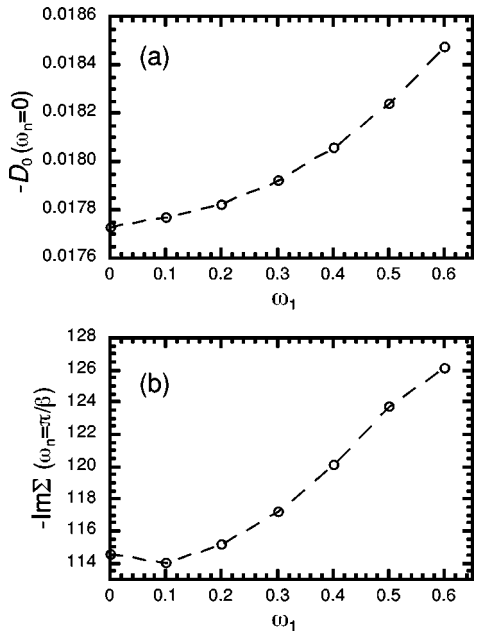

FIG. 5. Results for the dispersive boson model in the atomic regime with $\omega_0=8$ and $U=9$ ($\lambda=24$) at $\beta=8$; (a) the bare impurity Green's function for bosons at zero Matsubara frequency and (b) the imaginary part of the self-energy for fermions at the smallest Matsubara frequency. The lines are guides to the eye.

away from the antiadiabatic limit, that is, $U>W$ and $\omega_0 \sim W$. It is difficult to study this regime by any perturbative and analytical approach because of strong fluctuations. Our DMF method including fluctuation effects is applied to this nonperturbative regime without any difficulty.

Figure 6 shows the results for $\omega_0=0.5$ and $U=2.56$ ($\lambda=0.8$). As shown in Fig. 6(a), the absolute value of the bare impurity Green's function for bosons $\mathcal{D}_0$ decreases as ω_1 increases. The imaginary part of the self-energy for fermions also decreases in absolute value as shown in Fig. 6(b). At the same time, the probability of double occupancy P_{D} decreases from 1/2 as shown in Fig. 6(c). Figure 6(d) shows that the double-peak structure of the probability $P(x)$ becomes unclear, merging into a single peak. All these features show that the effective interaction between fermions U_{eff} is weakened and the polaron state becomes unstable for ω_1. This is a striking contrast to the previous results in Secs. III C and III D. We will discuss a physical picture for this behavior in Sec. IV.

In the intermediate region, we find a crossover as the value of ω_1 increases. Figure 7 shows this crossover for $\omega_0=0.5$ and $U=0.64$ ($\lambda=0.4$). For small values of ω_1, we find a similar behavior as seen in Fig. 4; the bare impurity Green's function for bosons is enhanced and both the absolute value of the self-energy and the double occupancy increase as ω_1. However, for $\omega_1 \gtrsim 0.2$, the behavior is reversed; all three quantities begin to decrease as in Fig. 6. Therefore in this intermediate region, as the value of ω_1 increases, the effective interaction between fermions is enhanced for small values of ω_1, but begins to be weakened for large values of ω_1.

This crossover is closely related to complete softening of the boson field. Figure 8 shows the effective frequency of the boson field ω^*, given by a pole of the Green's function for bosons as

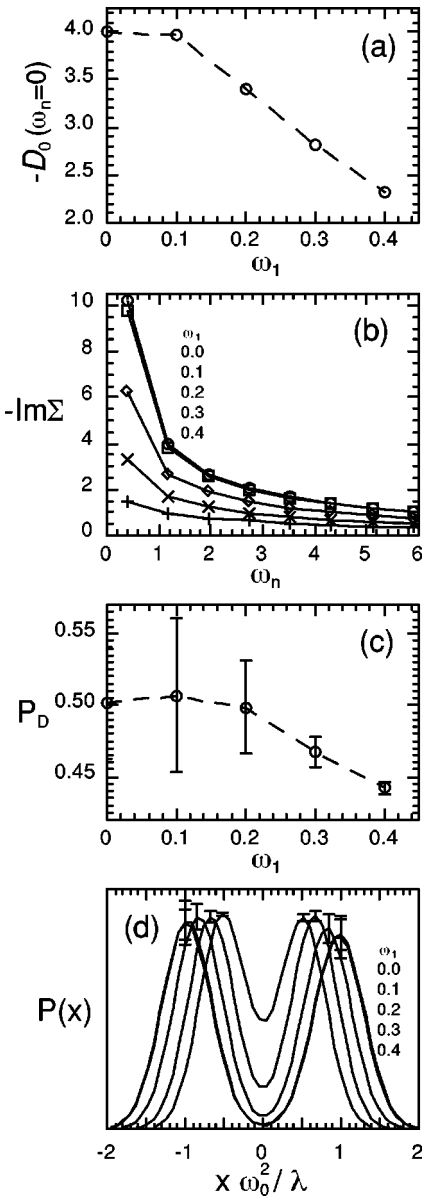

FIG. 6. Results for the dispersive boson model with $\omega_0=0.5$ and $U=2.56$ ($\lambda=0.8$) at $\beta=8$; (a) the bare impurity Green's function for bosons at zero Matsubara frequency, (b) the imaginary part of the self-energy for fermions, (c) the probability of double occupancy, and (d) the probability function of the boson fields x. The lines in (a)–(c) are guides to the eye. In (d), the typical error bars are shown at the peaks of the distributions.

$$\omega^*=\sqrt{(\omega_0-\omega_1)^2+\Pi(i\omega_n=0)}, \tag{23}$$

where Π is the self-energy for bosons. The frequency ω^* goes to zero at the value of ω_1 where the crossover from enhancement to weakening of the effective interaction is exhibited in Fig. 7.

F. Phase diagram

We systematically investigate the crossover found in the previous section by changing the parameters ω_0 and U. Figure 9 shows the values of ω^* as a function of U for the cases of (a) $\omega_0=0.5$ and (b) $\omega_0=2.0$, for instance. For finite values of the width ω_1, the frequency ω^* goes to zero in both

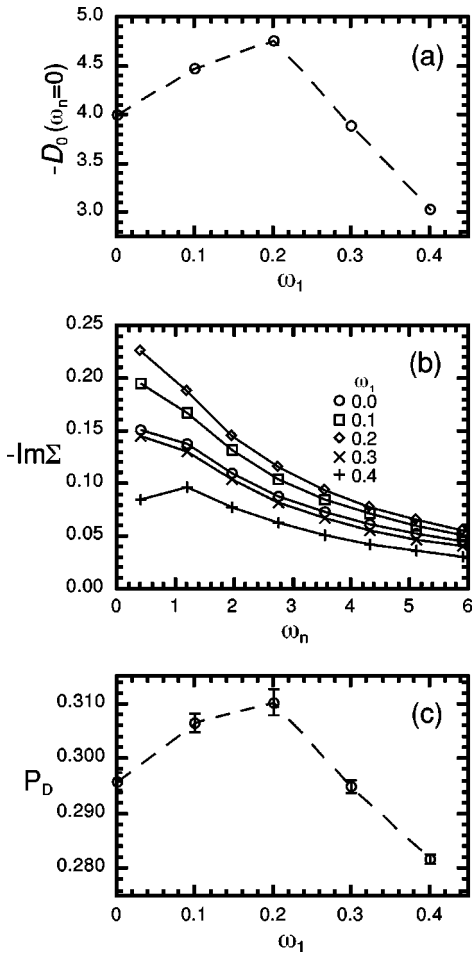

FIG. 7. Crossover in the intermediate coupling region with $\omega_0=0.5$ and $U=0.64$ ($\lambda=0.4$) at $\beta=8$; (a) the bare impurity Green's function for bosons at zero Matsubara frequency, (b) the imaginary part of the self-energy for fermions, and (c) the probability of double occupancy. The lines are guides to the eye.

cases. We determine the crossover values of U for different values of ω_0 and ω_1 by this complete softening of ω^*.

Figure 10 summarizes the phase diagram for the crossovers determined by the above criterion. This identifies the boundary between the weak-fluctuation and strong-fluctuation regimes as discussed in Sec. IV. The most important point in this phase diagram is that, especially for large ω_0, the energy scale of U for this crossover is quite different from U^* determined in Sec. III B. This suggests that there is another parameter that controls the onset of strong fluctuations as discussed in the next section.

IV. DISCUSSION

In this section, we discuss the results obtained in Sec. III. Perturbative arguments are applied to discuss the enhancement of the effective interaction between fermions in the weak-coupling[4] and atomic regions.[5,6,1] In the strong-coupling regime away from the antiadiabatic limit, the weakening of the effective interaction and the instability of the polaron state are discussed as a consequence of the strong fluctuations of the boson fields accompanied by complete softening. The phase diagram is examined to clarify the parameters that control the onset of the strong fluctuations.

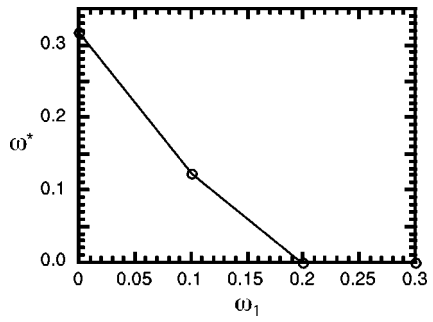

FIG. 8. The effective frequency of bosons in the case of $\omega_0=0.5$ and $U=0.64$ at $\beta=8$. The line is a guide to the eye.

In the weak-coupling region, the dispersion width ω_1 enhances the effective interaction between fermions in our DMF solutions. The absolute value of the self-energy for fermions is enhanced. A first-order perturbation in the coupling parameter λ shows that the self-energy Σ becomes larger as the width ω_1 increases since $\mathcal{D}_0$ increases as ω_1.[4] Thus, perturbation theory suggests that the boson dispersion increases the effective interaction between fermions in the weak-coupling limit. This enhancement can be understood intuitively as follows: In the weak-coupling region, the densities of states for both fermions and bosons are not altered drastically by the fermion-boson interaction; a rigid-band picture should be justified. For a finite ω_1, the band edge of the boson density of states is lowered linearly. Then the effective interaction (14) is mainly mediated by the bosons near the band edge as

$$U_{\mathrm{eff}}(i\omega_n)\sim\frac{\lambda^2}{(i\omega_n)^2-(\omega_0-\omega_1)^2}. \tag{24}$$

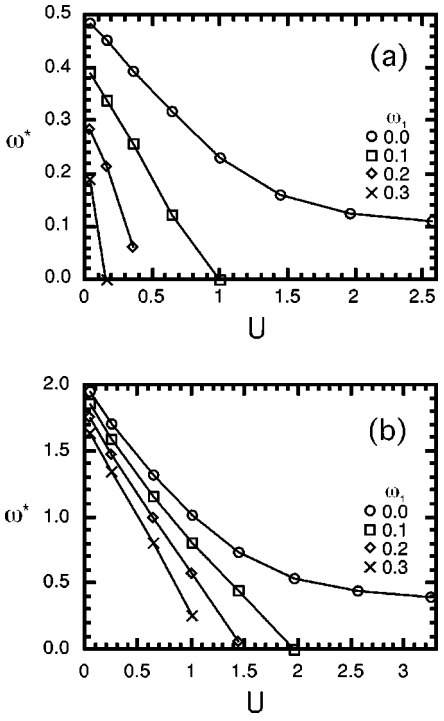

FIG. 9. The softening of the effective boson frequency for (a) $\omega_0=0.5$ and (b) $\omega_0=2.0$ at $\beta=8$. The lines are guides to the eye.

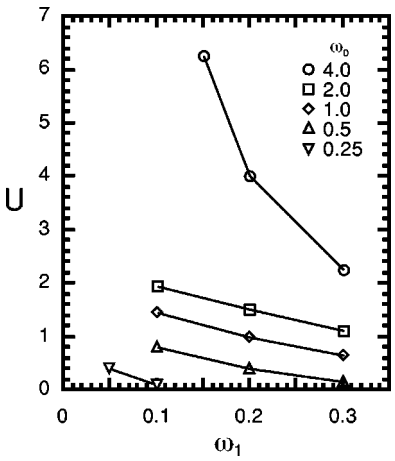

FIG. 10. The phase diagram of the crossover for various values of ω_0. The boundaries are determined by the complete softening of the effective boson frequency. The lines are guides to the eye.

Thus the absolute value $|U_{\mathrm{eff}}|$ becomes large as the value of ω_1 increases. Therefore, the enhancement of the effective interaction in the weak-coupling region can be understood as a decrease of the effective boson frequency. Our results in Sec. III C are consistent with this perturbative argument.

We now turn to the atomic limit, $W\ll\omega_0$ and U. Now the fermion hopping term in Eq. (7) is a perturbation to the terms (8) and (9). If we apply the canonical transformation to diagonalize the unperturbed terms according to small polaron theory,[5,6,1] we obtain the expression of the Hamiltonian as

$$\mathcal{H}=\mathcal{H}_{\mathrm{B}}-\sum_{i\alpha}c_{i\alpha}^{\dagger}c_{i\alpha}\Delta+\sum_{ij,\alpha}t_{ij}c_{i\alpha}^{\dagger}c_{j\alpha}X_i^{\dagger}X_j, \tag{25}$$

where Δ is the stabilization energy of polarons given by

$$\Delta=\sum_{\mathbf{q}}\frac{\lambda^2}{\omega_{\mathbf{q}}}, \tag{26}$$

and the operator X_i takes the form

$$X_i=\exp\left[-\mathrm{i}\sum_{\mathbf{q}}e^{\mathrm{i}\mathbf{q}\cdot\mathbf{r}_i}\frac{\lambda}{\omega_{\mathbf{q}}}\sqrt{\frac{2}{M\omega_{\mathbf{q}}}}p_{\mathbf{q}}\right]. \tag{27}$$

The third term of the Hamiltonian (25) indicates that the hopping occurs not as a bare fermion but as a combined object between fermions and bosons. Each fermion is associated with local bosons. This is called the small polaron state.

In the unperturbed state ($t_{ij}=0$), the polarons are almost localized in real space with the stabilization energy Δ given by Eq. (26). When one increases the width of the boson dispersion ω_1, the stabilization energy Δ increases. This makes the polarons more strongly localized. The delocalization of the polarons is a second-order perturbation in t terms in Eq. (25) since the polarons correspond to double occupancy of fermions in this model. The hopping matrix by second-order processes is suppressed by ω_1 because the intermediate state in the perturbation costs energy Δ. The operator X_i does not change the result in this limit of $\omega_0\gg W$. Therefore, the finite width of the boson dispersion suppresses the band motion of the polarons and enhances the effective

interaction in this limit. Our results in Sec. III D are in good agreement with this argument based on small polaron theory.

We now discuss the strong-coupling regime away from the antiadiabatic limit studied in Sec. III E. In this regime, the polaron state is formed by strong coupling; however, the boson fields are loosely bound to the fermions due to a finite ω_0, compared to the previous atomic limit with $\omega_0 \gg W$, where the boson fields react instantaneously to fermion motions. This leads to large fluctuations in the boson fields caused by the hopping of fermions. These fluctuations may in turn accelerate the delocalization of fermions through the mutual feedback effects of the fermion-boson coupling. Thus this regime is characterized by these strong fluctuations, which is the reason why a perturbation cannot be applied.

The finite width of the boson dispersion ω_1 introduced in our calculations increases the fluctuations of the boson fields. The bosons are not localized and gain their kinetic energy through dispersion. By tuning the width ω_1, we can control the fluctuations of the boson fields by hand. Our results in Sec. III E clearly exhibited that the effective interaction between fermions is weakened by ω_1. This is considered to be a consequence of the strong fluctuations of the boson fields enhanced by ω_1, which tend to make fermions more delocalized. This behavior is elucidated by our method, which fully includes the mutual feedback in many-body systems.

In the intermediate region, a sharp crossover was found by changing the value of ω_1 in Sec. III E. For small ω_1, the effective interaction is enhanced by ω_1. Since the fluctuations are small there, this may be smoothly connected to the behavior discussed in the weak-coupling or atomic regions. The effective frequency ω^* defined by Eq. (23) becomes small but remains finite as in the perturbative regime, although the reduction of ω^* is large and nonlinear in this nonperturbative regime. When the value of ω_1 becomes large enough to soften the boson field completely ($\omega^* \to 0$), fluctuations play a crucial role in enhancing the delocalization of fermions. Therefore the boundaries in the phase diagram in Fig. 10 are the crossovers between the weak-fluctuation and strong-fluctuation regimes. The latter regime is characterized by the weakening of the effective interaction between fermions by the dispersive bosons, which soften completely.

In the dispersionless case in Sec. III B, we found another crossover caused by the formation of bipolarons, which is characterized by the development of the double-peak structure in the probability $P(x)$. The critical value of U for this crossover, U^*, changes from $U^* \sim 3$ in the limit of $\omega_0 \gg W$ (antiadiabatic limit) to $U^* \sim 1$ in the limit of $\omega_0 \ll W$ (adiabatic limit) as shown in the schematic phase diagram in the plane $(1/\omega_0, U)$ in Fig. 11 (dotted gray line). On the other hand, the crossover to the strong-fluctuation regime in Fig. 10 appears at much larger values of U than U^*, especially in the antiadiabatic regime with large but finite ω_0. This strongly suggests the importance of another energy scale in characterizing the strong-fluctuation regime which is not found in our calculations for the dispersionless case.

The importance of such a characteristic energy scale was also pointed out in a previous mean-field study.[29] The parameter is defined by the ratio of the fermion-boson interaction to the spring constant of the boson fields, $\eta = \lambda / M\omega_0^2$. In the case of $\eta < 1$, since the fermion-boson interaction is weak compared to the stored energy in the boson field, single-boson processes should be important. In the case of $\eta > 1$, the fermion-boson interaction is strong enough to excite a large numbers of bosons, i.e., multiboson processes become important. The previous study[29] suggested the importance of fluctuations of the boson fields in the latter multiboson regime.

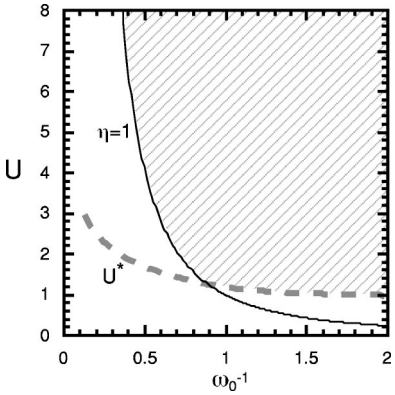

FIG. 11. Schematic phase diagram for the dispersionless case. The critical value for the formation of the small polaron state U^* is shown as the dotted gray line. The solid line indicates the boundary $\eta = 1$. The hatched area is the strong-fluctuation region. See the text for details.

In the plane $(1/\omega_0, U)$, the crossover $\eta = 1$ between the single-boson and multiboson regimes corresponds to $U = \omega_0^2$ as shown in Fig. 11 (solid line). The line of $\eta = 1$ becomes much larger than U^* in the antiadiabatic regime. If we plot these values of $U(\eta = 1)$ on the axis of $\omega_1 = 0$ in Fig. 10, the crossover boundaries seem to be smoothly extrapolated to these values in the antiadiabatic region. We demonstrate this behavior in Fig. 12 for $\omega_0 = 4$ and 2 (gray lines). This indicates that in the antiadiabatic regime the line of $\eta = 1$ corresponds to the crossover between the weak-fluctuation and strong-fluctuation regimes in the dispersionless case.

On the other hand, in the adiabatic regime with small but finite ω_0, the value of U for the boundary in Fig. 10 is not

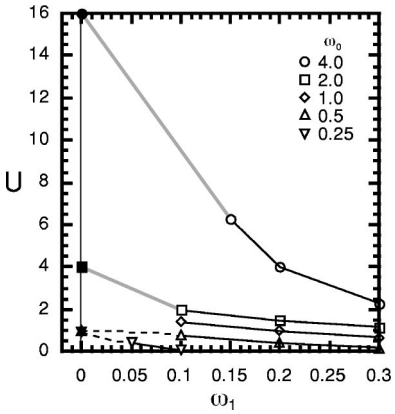

FIG. 12. The values of U and ω_1 at which the crossover from the weak-fluctuation to the strong-fluctuation regime takes place. Notice that these values extrapolate smoothly to the values of U at $\eta = 1$ for $\omega_0 = 4$ and 2 (antiadiabatic regime) and to U^* for $\omega_0 = 0.5$ and 0.25 (adiabatic regime) in the limit of $\omega_1 = 0$. See the text for details.

smoothly connected to the value of U for $\eta=1$. For instance, in the case of $\omega_0=0.5$, $\eta=1$ gives $U=1/4$, which is much smaller than the boundary value. This suggests that the condition of $\eta>1$ does not characterize the strong-fluctuation regime in this adiabatic region.

To understand this behavior in the adiabatic regime, let us discuss the adiabatic limit of $\omega_0\to 0$. In this limit, the boson fields behave as classical fields which do not fluctuate in the imaginary time direction. Boson fluctuations come only from the fluctuation of the value of the field x, which is constant in time. Thus, even if the system is in the region of $\eta>1$, the fluctuations of the boson fields are small when U is smaller than U^*, since the fields experience a deep single-well potential as indicated in the probability $P(x)$. The boson fields begin to fluctuate when U becomes comparable to U^*, where the potential for x softens around $x=0$. Therefore in the adiabatic limit, the strong-fluctuation regime should be characterized not by $\eta>1$ but by $U>U^*$.

Based on this argument, if we plot the value of U^* on the axis of $\omega_1=0$ in the adiabatic regime, the crossover boundaries seem to be smoothly extrapolated to these values. Figure 12 exhibits this behavior for the cases of $\omega_0=0.5$ and 0.25 (dashed lines).

These results show that boson fluctuations that are strong enough to accelerate the delocalization of fermions appear in a different way in the antiadiabatic and adiabatic regimes. In the antiadiabatic regime ($\omega_0>W$), the bipolaron state is formed at $U\gtrsim U^*$. In the region with $U>U^*$ and $\eta<1$, however, the fluctuations of the boson fields are small in the sense that the single-boson process is the main contributor and the effective boson frequency is finite. If η becomes larger than 1, the boson field is softened and the boson fluctuations play a crucial role through multiboson processes. On the other hand, in the adiabatic regime ($\omega_0<W$), the fluctuations do not become large until $U\sim U^*$ even if η is larger than 1. The fluctuations are mainly of classical origin there.

To summarize, strong fluctuations of the boson fields become important only when the conditions $U>U^*$ and $\eta>1$ are both satisfied. These conditions are shown as the hatched area in Fig. 11. This area is the strongly correlated region for both fermions and bosons. The criterion for the formation of bipolarons, $U\sim U^*$, corresponds to a competition between the kinetic energy of fermions W and the effective interaction U.[30] On the other hand, the criterion $\eta\sim 1$ corresponds to a competition between the stored energy of the boson field and the coupling energy to fermions. Thus the hatched area in Fig. 11 is the region where correlations become strong from the standpoint of both fermions and bosons.

We note that the fluctuation effects are most conspicuous near the boundaries $U=U^*$ and $\eta=1$ in the hatched area in Fig. 11. The reduction of $|\mathcal{D}_0|$ and $|\mathrm{Im}\Sigma|$ becomes smaller when the system goes away from these boundaries. It is quite reasonable that the polaron state becomes stable when it is less affected by fluctuations away from the boundaries. This has been indicated by a mean-field study[29] and also by a Monte Carlo study of the single-fermion problem.[31,32] Even though the magnitude of the fluctuation changes, it should be stressed that its role in the hatched area in Fig. 11 differs essentially from the perturbative regime described above.

The criteria $U>U^*$ and $\eta>1$ have been discussed for the formation of the small polaron in a system with a single fermion interacting with a boson field.[33,34] In the single-fermion problem, the boson field is not affected by fermion-boson coupling in the thermodynamic limit. There is no feedback to bosons from changes of the fermion state. In other words, the self-energy for bosons is always zero. The present study successfully describes such feedback effects in many-body fermion systems.

A subtle problem remains open concerning the boson softening in the dispersionless case. As shown in Fig. 9, when ω_1 is zero, the effective frequency ω^* becomes very small but remains finite for large values of U. We note that there are finite-temperature effects; ω^* is more suppressed for lower temperatures. Unfortunately we cannot conclude from this study whether ω^* goes to zero even when $\omega_1=0$. In this dispersionless case, the boson density of states is a δ function at $\varepsilon=\omega_0$, which is a special case since the shape of the boson density of states at the bottom is important, as mentioned in Sec. III A. For instance, a steplike singularity in the two-dimensional density of states might prevent the boson field from complete softening at finite temperatures. Although further studies are necessary of the properties of DMF equations for various types of density of states, we believe from the results in Figs. 11 and 12 that even when $\omega_1=0$ the nonlinear suppression of ω^* is relevant to strong fluctuations of bosons and that there are two important energy scales.

V. SUMMARY AND CONCLUDING REMARKS

We have investigated the effects of boson dispersion in a system of dynamical mean-field equations describing coupled fermion-boson systems. The analysis of the equations revealed that the boson dispersion plays a crucial role in a wide region of parameters. By introducing a parameter for the width of the dispersion in the model, we can control the fluctuations of the boson fields. To handle the boson fluctuations and the feedback effects, we have extended the dynamical mean-field theory to determine the Green's functions for both fermions and bosons in a self-consistent way. In the ordinary framework for the dispersionless case, the channel for the boson Green's function is frozen in the sense that the bare impurity Green's function is fixed and unrenormalized from the noninteracting one. The renormalization of the bare impurity Green's function for bosons is very important since the bare impurity Green's function is directly related to the effective interaction between fermions. The equations in extended dynamical mean-field theory are solved by using the quantum Monte Carlo technique.

The main result in models with dispersive bosons is that in the strong-coupling regime away from the antiadiabatic limit the fluctuations of the boson fields become relevant in accelerating the delocalization of fermions. The effective interaction between fermions is weakened as the width of the boson dispersion increases in this regime. This behavior is explicitly shown by our method, which fully includes the mutual feedback effects in many-body systems. The crossover to this nonperturbative regime is closely correlated with softening of the boson field. We have examined the phase diagram where this strong fluctuation occurs by tuning the coupling parameter and the width of the dispersion. The

strong fluctuations that delocalize fermions become relevant when the bipolaron state is formed and multiboson processes become important. The bipolarons become stable when the effective interaction between fermions overcomes the fermion band energy. The multiboson regime is characterized by a coupling parameter larger than the boson energy. Thus the strong-fluctuation regime is the strongly correlated region for both fermions and bosons. As the coupling parameter increases, the boson fluctuations accompanied by the softening of the boson fields appear in a different way in the adiabatic and the antiadiabatic regimes. In the adiabatic regime, the fluctuations are mainly classical and are enhanced by the softening of the potential for the boson fields in the formation of the small polaron state. On the other hand, in the antiadiabatic regime, the bipolarons are formed in the single-boson regime, where the dynamical fluctuations are small and the effective boson frequency is finite. The boson fluctuations do not play a crucial role until the system enters the multiboson regime by complete softening of bosons.

The onset of the strong fluctuations occurs near the region where the boson degrees of freedom soften. In this paper we have studied the dynamical mean-field equations in the absence of any freezing of the boson degrees of freedom. These effects together with generalizations to states with different symmetries and other generalizations are currently under investigation.

Our results imply that the behavior of the boson fluctuations may depend on the specific form of the boson density of states. Different forms of the density of states should be tested in the present dynamical mean-field framework in a future study. In particular, we are interested in the two-dimensional case with a steplike singularity at the edge, which might be free from complete softening at finite temperatures. Boson fluctuations in this case may lead to light-mass bipolaronic states, which would give some insights into the high temperature superconductivity in Cu oxide materials where fermions strongly couple with spin fluctuations. We plan to examine this two-dimensional case in a later publication.

The dynamical mean-field equations allow us to vary the width of the boson dispersion in the calculations. This reveals interesting properties in the strong-fluctuation regime. Tuning of the electronic bandwidth has been the subject of a great deal of theoretical and experimental work.[35] Our work suggests the possible interest of varying the boson dispersion experimentally. This may be easier in systems where the bosons are spin fluctuations whose dispersion (determined by exchange interactions) can be controlled more easily than optical phonon dispersions. Another possibility may be the realization of the dynamical mean-field theory in a random model.

There are many materials that satisfy the above conditions for the strong-fluctuation regime. In many physical situations, the fermion bandwidth W is large or comparable to ω_0, which makes it possible to access the strong-fluctuation regime by a relatively weak coupling. Our method provides a powerful theoretical tool for examining the physical properties in this regime. We can apply it to more realistic models including orbital degrees of freedom of electrons, different normal modes of phonons, or interactions between fermions. Such extensions are now under investigation.

ACKNOWLEDGMENTS

Y.M. acknowledges the financial support of the Japan Society for the Promotion of Science for Young Scientists. G.K. is supported by the NSF under Grant. No. DMR 95-29138.

[1] G. D. Mahan, *Many Particle Physics* (Plenum Publishing, New York, 1981), and references therein.
[2] J. Hubbard, Phys. Rev. Lett. **3**, 77 (1959).
[3] R.L. Stratonovich, Dokl. Akad. Nauk (SSSR) **115**, 1097 (1957) [Sov. Phys. Dokl. **2l**, 416 (1957)].
[4] A.B. Migdal, Zh. Éksp. Teor. Fiz. **34**, 1438 (1958) [Sov. Phys. JETP **7**, 996 (1958)].
[5] T. Holstein, Ann. Phys. (N.Y.) **8**, 325 (1959).
[6] T. Holstein, Ann. Phys. (N.Y.) **8**, 343 (1959).
[7] A. Georges, G. Kotliar, W. Krauth, and M.J. Rozenberg, Rev. Mod. Phys. **68**, 13 (1996), and references therein.
[8] Q. Si, J.L. Smith, and K. Ingersent, cond-mat/9905006 (unpublished).
[9] R. Chitra and G. Kotliar, cond-mat/9903180 (unpblished).
[10] J. Robin, A. Romano, and J. Ranninger, cond-mat/9808252 (unpublished).
[11] Y. Motome and M. Imada, Phys. Rev. B **60**, 7921 (1999).
[12] H. Nakano, Y. Motome, and M. Imada, J. Phys. Soc. Jpn. **69**, 1282 (2000).
[13] A.P. Ramirez, P. Schiffer, S.-W. Cheong, W. Bao, T.T.M. Palstra, P.L. Gammel, D.J. Bishop, and B. Zegarski, Phys. Rev. Lett. **76**, 3188 (1996).
[14] C.H. Chen, S.-W. Cheong, and H.Y. Hwang, J. Appl. Phys. **81**, 4326 (1997).
[15] S. Mori, C.H. Chen, and S.-W. Cheong, Nature (London) **392**, 473 (1998).
[16] M.T. Fernández-Díaz, J.L. Martínez, J.M. Alonso, and E. Herrero, Phys. Rev. B **59**, 1277 (1999).
[17] J.E. Hirsch and E. Fradkin, Phys. Rev. Lett. **49**, 402 (1982).
[18] J.E. Hirsch and E. Fradkin, Phys. Rev. B **27**, 4302 (1983).
[19] R.T. Scaletter, N.E. Bickers, and D.J. Scalapino, Phys. Rev. B **40**, 197 (1989).
[20] R.M. Noack, D.J. Scalapino, and R.T. Scaletter, Phys. Rev. Lett. **66**, 778 (1991).
[21] J.K. Freericks, M. Jarrell, and D.J. Scalapino, Phys. Rev. B **48**, 6302 (1993).
[22] A.J. Millis, R. Mueller, and B.I. Shraiman, Phys. Rev. B **54**, 5389 (1996).
[23] J.E. Hirsch and R.M. Fye, Phys. Rev. Lett. **56**, 2521 (1986).
[24] The QMC calculation becomes difficult for very small values of ω_0.
[25] K. Takegahara, J. Phys. Soc. Jpn. **62**, 1736 (1992).
[26] R. Micnus, J. Ranninger, and S. Robaszkiewics, Rev. Mod. Phys. **62**, 113 (1990), and references therein.
[27] P.G.J. van Dongen, Mod. Phys. Lett. B **5**, 861 (1991).
[28] P.G.J. van Dongen, Phys. Rev. B **45**, 2267 (1992).
[29] D. Feinberg, S. Ciuchi, and F. de Pasquale, Int. J. Mod. Phys. B **4**, 1317 (1990).

[30] The line of U^* may be modified according to the specific form of the fermion-boson coupling.
[31] H. de Raedt and A. Lagendijk, Phys. Rev. B **27**, 6097 (1983).
[32] H. de Raedt and A. Lagendijk, Phys. Rev. B **30**, 1671 (1984).
[33] M. Capone, W. Stephan, and M. Grilli, Phys. Rev. B **56**, 4484 (1997).
[34] S. Ciuchi, F. de Pasquale, S. Fratini, and D. Feinberg, Phys. Rev. B **56**, 4494 (1997).
[35] M. Imada, A. Fujimori, and Y. Tokura, Rev. Mod. Phys. **70**, 1039 (1998), and references therein.